PULSE POSITION PRE-CODING EXPLOITING UWB POWER CONSTRAINTS

Florian Troesch, Frank Althaus, and Armin Wittneben

Swiss Federal Institute of Technology (ETH) Zurich
Communication Technology Laboratory, CH-8092 Zurich, Switzerland
Email: {troesch,althaus,wittneben}@nari.ee.ethz.ch

ABSTRACT

Due to dense multipath channels, coherent receivers in *Ultra-Wideband Impulse Radio* (UWB-IR) technology are high in hardware complexity and power consumption. This makes coherent receivers in downlink transmission of *Low Data Rate* (LDR) applications, where a more complex node communicates with many basic sensors, unreasonable. Pre-coding schemes are known solutions to transfer receiver complexity to transmitter side, while maintaining receiver performance. We sketch performance and scalability potential of pre-coding schemes in LDR systems in presence of drastic *Federal Communications Commission's* (FCC) power constraints. This is done by *Symbol Error Rate* (SER) analysis of an easily realizable *Pulse Position Pre-coding* (PPP) scheme, supported by simulation results over measured UWB channels. Under realistic conditions, PPP gains up to $9\,\mathrm{dB}$ are demonstrated, and it is shown that already a few PPP pulses are sufficient to significantly reduce receiver complexity, at the expense of more transmit power.

1. INTRODUCTION

One characteristic that makes *Ultra-Wideband Impulse Radio* (UWB-IR) an interesting candidate for future indoor wireless communication is its extreme system scalability. While scalability with respect to transmission rate, bandwidth and coverage is inherent in UWB-IR system definition, we extend scalability with respect to a tunable trade-off between transmitter and receiver complexity (Tx/Rx-scalability).

UWB-IR transmitters produce very short time domain pulses of up to $7.5\,\mathrm{GHz}$ bandwidth without the need for an additional *Radio Frequency* (RF) mixing stage due to their essentially baseband nature. This leads to significant complexity reduction with respect to conventional radio systems at transmitter and receiver side. This advantage makes UWB-IR a well suited candidate for low cost *Low Data Rate* (LDR) applications. On the other hand, channel investigations [1] show that UWB-IR indoor channel energy is spread over a large number of multipath components. This highly increases complexity of coherent receivers as energy has to be recombined by a large number of RAKE fingers.

In low cost LDR systems, where a central more complex *Cluster Head* (CH) communicates with many basic *Sensor Nodes* (SN), application of coherent receivers in downlink communication is unreasonable. Hence, Tx/Rx-scalability would be very desirable. Non-coherent receivers are one proposed solution [2] to this problem, but they suffer from significant performance losses. Transmitter based channel equalization [3], Pre-RAKE [4, 5] or Time-Reversal [6] schemes are known solutions to maintain receiver performance, while transferring receiver complexity to transmitter side. These sophisticated pre-coding schemes seem to be too hardware consuming even for CH realizations. Furthermore, UWB-IR systems are intended to operate over a large bandwidth overlaying bands of many other services. They are rigorously power constrained by regulations, as e.g., by the *Federal Communications Commission* (FCC), to minimize interference to victim receivers. Considering FCC or FCC-like power constraints, it is even questionable, if mentioned UWB-IR pre-coding schemes show good performances at all, as they might violate peak power constraint.

In this paper, we investigate UWB-IR scalability potential in LDR systems with symbol rates below $300\,\mathrm{kHz}$, if drastic FCC power constraints have to be respected. This is done by *Symbol Error Rate* (SER) performance analysis of an easily realizable *Pulse Position Pre-coded Binary Pulse Position Modulated* (PPP-BPPM) transmit scheme with coherent *Selective RAKE* (SRAKE) receiver, which collects only a few of the strongest multipaths components. Results shown incorporate SER simulations using UWB channels from two different measurement campaigns, i.e., one in an office building and one in an industrial hall.

The applied PPP-BPPM scheme equals an orthogonal BPPM scheme of *equivalent pulses*, where each equivalent pulse consists of pulse position pre-coded copies of a basic pulse waveform. PPP is done by simply adjusting delays between the basic pulse waveforms such that either the strongest positive or negative paths of the channel add up coherently at the receiver. The transmitter adapts neither amplitudes nor polarity of the pulses to the channel, requiring only partial *Channel State Information* (CSI). This is assumed to be perfectly known by the transmitter. Furthermore, we allow the transmitter to use *as much power as admitted* by the FCC, as we are interested in maximum system scalability and consider FCC-like power constraints as binding enough.

In the next section, we introduce the system model of PPP-BPPM. In Section 3, we derive minimal temporal pre-coding distance and maximal number of allowed pre-coding pulses, directly from FCC power constraints. In Section 4, we present maximally achievable pre-coding gains as well as system scalability of PPP-BPPM, and demonstrate significant potential with respect to receiver complexity reduction. In Section 5, we conclude with a short summary.

2. SYSTEM MODEL

2.1. PPP-BPPM Transmitter

The PPP-BPPM signal sent by the transmitter is described by:

$$s_{tx}^{N_P}(t) = \sqrt{E_p} \sum_{k=-\infty}^{\infty} \sum_{n=0}^{N_P-1} w_{tx}(t - kT_f - a_k\delta - \tau_{p,n}), \quad (1)$$

where t is the transmitter's clock time and $w_{tx}(t)$ the real transmitted bandpass pulse of width T_w. The pulse is energy normalized, i.e., $\int_{-\infty}^{\infty} w_{tx}^2(t)dt = 1$, and E_p is the single pulse energy. During each frame repetition time T_f, one BPPM symbol a_k is transmitted. Depending on $a_k \in \{0, 1\}$, a sequence of N_P pre-coded pulses is either transmitted at beginning of the frame or delayed by δ. The frame repetition rate $R_f = 1/T_f$ equals the nominal BPPM pulse rate. The pre-coding delays $\tau_{p,0} < \tau_{p,1} < \ldots < \tau_{p,N_P-1}$ are chosen such that the N_P strongest multipath components of the channel add up coherently at the receiver. To avoid intersymbol interference between consecutive symbols and to maintain PPM orthogonality in presence of large channel excess delay τ_c, conditions $\delta \geq \tau_{p,N_P-1} + \tau_c + T_w$ and $T_f \geq \delta + \tau_{p,N_P-1} + \tau_c + T_w$ are respected. For simplicity, we consider peer-to-peer communication, only, and therefore omit pseudo-random time-hopping.

2.2. Coherent Receiver and Symbol Error Rate Analysis

The coherent SRAKE receiver applied for PPP-BPPM is the same as the one for BPPM [7] except that it selects the strongest paths from an equivalent channel which consists of the real channel convolved with the pre-coded frame. The SRAKE comprises two identical branches of N_R fingers, each, one adjusted to frame beginning ($a_k = 0$) and one delayed by δ ($a_k = 1$). Each finger equals a receive pulse matched filter $w_{rx}(-t)$, with $\int_{-\infty}^{\infty} w_{rx}^2(t)dt = 1$, tuned to a certain multipath component by delay $\tau_{r,i}$ and is weighted by a factor g_i, $i \in \{0, \ldots, N_R - 1\}$. The N_R sampled finger outputs of each branch are summed up to $r_k^{(0)}$ and $r_k^{(1)}$, respectively, followed by a maximum likelihood detector.

The received waveform at the output of the channel may be expressed as:

$$s_{rx}^{N_P}(t) = \sqrt{E_p} \sum_{k=-\infty}^{\infty} \sum_{n=0}^{N_P-1} h_w(t - kT_f - a_k\delta - \tau_{p,n}), \quad (2)$$

where $h_w(t) = w_{rx}(t) * h(t)$ is the convolution of the receive pulse $w_{rx}(t)$ and the real channel $h(t)$, which is assumed to be static over one frame.

For SER evaluation, we consider only the k-th frame and omit index k for convenience. Assuming perfect synchronization between transmitter and receiver, the sampled matched filter output of the i-th finger in the branch matched to symbol 0 (assuming 0 was sent) equals:

$$y_i^{(0)} = \sqrt{E_p} \sum_{n=0}^{N_P-1} h_{ww}(\tau_{r,i} - \tau_{p,n}) + n_{w,i}^{(0)} \quad (3)$$

$$= \sqrt{E_p} h_E(\tau_{r,i}) + n_{w,i}^{(0)} = h_{E,i} + n_{w,i}^{(0)}, \quad (4)$$

with $h_{ww}(t) = w_{rx}(-t) * h_w(t)$. The term $n_{w,i}^{(0)}$ equals the convolution $w_{rx}(-t) * n^{(0)}(t)$, sampled at time $\tau_{r,i}$, with $n^{(0)}(t)$ the real zero-mean Additive White Gaussian Noise from this branch. $n^{(0)}(t)$ has two-sided power spectral density equal to $N_0/2$. We call $h_E(t)$ the *equivalent pre-coded channel impulse response* and $h_{E,i}$ is a sample of $h_E(t)$ at time instance $\tau_{r,i}$.

The output of the SRAKE, if $a_k = 0$ was sent, is given by:

$$r = r^{(0)} - r^{(1)} = \sum_{i=0}^{N_R-1} g_i(y_i^{(0)} - n_{w,i}^{(1)}), \quad (5)$$

with g_i the weighting coefficient of the i-th finger, and $n_{w,i}^{(1)}$ the corresponding noise component from the branch matched to symbol 1. In order to avoid correlated noise samples $n_{w,i}^{(\alpha)}$, $\forall i$ and $\alpha \in \{0, 1\}$ at the SRAKE's output, we restrict the delays such that the pulse matched filters of the individual fingers are non-overlapping, i.e., $\tau_{p,i} \geq T_w + \tau_{p,i-1},\ i = 1, \ldots, N_R - 1$. The weighting coefficient g_i is chosen according to Maximum Ratio Combining, i.e., $g_i = h_{E,i}$. Finally, we have:

$$r = r_s + r_n = \sum_{i=0}^{N_R-1} \sqrt{E_p} h_{E,i}^2 + h_{E,i}(n_{w,i}^{(0)} - n_{w,i}^{(1)}), \quad (6)$$

with r_s the received signal component and r_n the sum of $2N_R$ independent zero-mean Gaussian random variables of variances $\sigma_i^2 = h_{E,i}^2(N_0/2)$. Hence, r_n is a zero-mean Gaussian random variable of variance $\sigma_r^2 = 2(N_0/2)\sum_{i=0}^{N_R-1} h_{E,i}^2$.

The maximum likelihood SER performance given a certain channel realization is now:

$$P_e = \frac{1}{2}\operatorname{erfc}\left(\sqrt{\frac{r_s^2}{2\sigma_r^2}}\right) = \frac{1}{2}\operatorname{erfc}\left(\sqrt{\frac{E_p\sum_{i=0}^{N_R-1} h_{E,i}^2}{2N_0}}\right). \quad (7)$$

By averaging P_e over different channel realizations, the SER can be determined.

3. AVERAGE AND PEAK POWER ANALYSIS

3.1. Maximal Average and Peak Power of Periodic Pulse Train

A device operating under FCC's provisions of UWB indoor devices [8], has to occupy a total 10 dB bandwidth of at least 500 MHz between 3.1 and 10.6 GHz. Additionally, the emitted signal has to respect average and peak power constraint. Average power P_{av} measurements are based on spectrum analyzers with *Resolution Bandwidth* (RBW) set to $B_{av} = 1\,\text{MHz}$, RMS detector and average time window $T_{aw} = 1\,\text{ms}$. For all center frequencies f_0 of the resolution filter between 3.1 and 10.6 GHz, maximal average power $P_{av}^{\max}$ has to be below $P_{av}^{\text{FCC}} = -41.25\,\text{dBm}$. Peak power, according to [8] and [9], is best measured with a RBW of $B_p = 50$ MHz. For all center frequencies f_0 within 3.1 to 10.6 GHz, maximal peak power $P_p^{\max}$ must not exceed $P_p^{\text{FCC}} = 0\,\text{dBm}$.

According to [9], maximal average and peak power of a periodic signal with equally spaced pulses, defined by $s(t) = \sqrt{E_p}\sum_{n=-\infty}^{\infty} w(t - n/R_f)$, can be approximated very tightly as:

$$P_{av}^{\max}(R_f, f_0) = \begin{cases} 2E_pW^2(f_0)B_{av}R_f & \frac{1}{T_{aw}} \leq R_f \leq B_{av} \\ 2E_pW^2(f_0)R_f^2 & R_f > B_{av} \\ & \text{and } f_0 = lR_f, \end{cases} \quad (8)$$

$$P_p^{\max}(R_f, f_0) = \begin{cases} \frac{2E_pW^2(f_0)B_p^2}{0.45^2} & R_f < \frac{B_p}{0.45} \\ 2E_pW(f_0)^2R_f^2 & R_f > \frac{B_p}{0.45} \\ & \text{and } f_0 = lR_f, \end{cases} \quad (9)$$

with $W(f)$ the Fourier transform of the normalized pulse waveform $w(t)$ and l any integer value. The condition $f_0 = lR_f$ arises from the period of the signal $s(t)$ and avoids center frequencies f_0 at which $P_{av}^{\max}$ and $P_p^{\max}$ are zero. The two regimes in (8) and (9) origin from the fact that for low frame repetition frequencies, resolution filtered pulses do not overlap and add up linearly in power, while for higher frequencies, they overlap and add up linearly in amplitude. Next, we set the maximal powers $P_{av}^{\max}$ and $P_p^{\max}$ equal to the maximally allowed powers P_{av}^{FCC} and

P_p^{FCC}, and solve for $E_p W^2(f_0)$. In so doing, maximally allowed single pulse spectral energy at frequency f_0 with respect to average and peak power constraint is achieved as shown in Fig. 1. Two

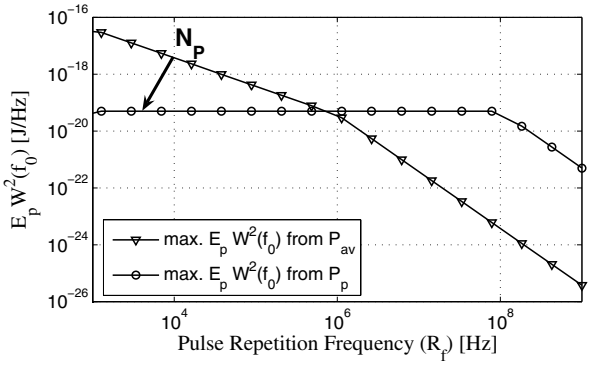

Fig. 1. Maximally allowed single pulse spectral energy with respect to peak and average power.

different regimes can be distinguished, i.e., peak power regime for $R_f < B_{av} = 1\,\text{MHz}$ and average power regime for $R_f > B_{av}$. From Fig. 1 and Eq. (9), it follows that peak power does not increase as long as $R_f < B_p/0.45$.

3.2. Impact of FCC Average and Peak Power Constraint on LDR PPP-BPPM

For the rest of the paper, LDR PPP-BPPM schemes with frame repetition rate $R_f \leq 300\,\text{kHz}$, BPPM modulation shift $\delta \leq 1/(2R_f)$, and minimal temporal pulse distance $T_{pc} \geq 10\,\text{ns}$ are considered, i.e., UWB-IR operating in peak power regime.

Under above system specifications, the uncoded LDR BPPM signal and the periodic one from previous section show approximately the same maximal average and peak power, if same R_f is applied [9]. For $R_f \leq 300\,\text{kHz}$, the resolution filtered pulses are non-overlapping for BPPM and the periodic signal. As the number of pulses that fall into the averaging time $T_{aw} = 1\,\text{ms}$ is approximately the same for both, average power is approximately equal. Peak power is unchanged as minimal temporal pulse distance is larger than $10\,\text{ns} > 0.45/B_p$. From same argumentation, it follows that PPP-BPPM with $T_{pc} \geq 10\,\text{ns}$ shows the same peak power as the corresponding periodic signal. For maximal PPP-BPPM average power, an accurate upper bound can be found assuming that each doubling of pre-coding pulses increases BPPM average power by 6 dB. This assumption is equivalent to assuming average power resolution filtered pulses as totally overlapping, and therefore, to add up perfectly in amplitude. As average power filtered pulses extend over about 2μs and are separated by only a few nanoseconds due to PPP, this is a reasonable assumption. Hence, maximal average and peak power of LDR PPP-BPPM of N_P pulses equals:

$$P_{av}^{\max}(R_f, f_0) = 2E_p W^2(f_0) B_{av} N_p^2 R_f \quad (10)$$

$$P_p^{\max}(R_f, f_0) = \frac{2E_p W^2(f_0) B_p^2}{0.45^2}, \quad (11)$$

and the maximally allowed single pulse spectral energies:

$$E_{p,av}^{\text{PPP}} W^2(f_0) = \frac{P_{av}^{\text{FCC}}}{2N_P^2 R_f B_{av}} \quad (12)$$

$$E_{p,p}^{\text{PPP}} W^2(f_0) = \frac{0.45^2 P_p^{\text{FCC}}}{2B_p^2}. \quad (13)$$

According to Fig. 1, FCC power constraints are fully exploited, if maximally allowed single pulse spectral energies in (12) and (13) are equal, i.e., if we increase average power to its maximally allowed value, while keeping peak power constant. By equating the two expressions and solving for N_P, maximal number of pre-coding pulses is found that can be applied without violating FCC power constraints:

$$N_P^{\max} = \left\lfloor \sqrt{\frac{1}{0.45^2 R_f} \frac{B_p^2}{B_{av}} \frac{P_{av}^{\text{FCC}}}{P_p^{\text{FCC}}}} \right\rfloor. \quad (14)$$

It is remarkable that (14) scales with $1/\sqrt{R_f}$, which is due to the fact that average power in (8) scales with R_f for $R_f \leq 1\,\text{MHz}$. Examples of (14) are: 2 pulses at 200 kHz, 3 at 100 kHz and 6 at 20 kHz. The number of pre-coding pulses that can be applied is quite restricted, all the same, significant performance improvement is possible as will be shown in the following section.

4. SIMULATION RESULTS

In this section, SER performance results for LDR PPP-BPPM schemes, with detailed specifications given in Section 3.2, are presented based on measured UWB *Channel Impulse Responses* (CIR) with bandwidth B from 500 MHz up to 7.5 GHz.

Most of used UWB channels are taken from a UWB measurement campaign performed at ETHZ [10] in a SPIN (Sensor, Positioning and Identification Network) or warehouse like scenario, i.e., in rich scattering environment similar to [11]. The equipment is restricted to a frequency range of 3 to 6 GHz. The receiver was placed on a tripod at fixed position in a big storage room, full of metallic objects, e.g., large metallic shelves. The transmit antenna was mounted on a two-dimensional positioner, which allowed for random walks in several *Line-Of-Sight* (LOS) and *Non-Line-Of-Sight* (NLOS) regions of $27\,\text{cm} \times 56\,\text{cm}$. A total of 4500 individual CIRs in 22 different areas were measured.

In order to demonstrate PPP-BPPM also over channels extending over the entire UWB bandwidth from 3.1 to 10.6GHz, we simulated also over channels taken from a measurement campaign at IMST [12]. These measurements were performed with a network analyzer of frequency range 1 to 11 GHz in an office building and were among others basis for well-known IEEE 802.15a channel model.

In Fig. 2, *Cumulative Distribution Functions* (CDF) of the energy at channel output are plotted as a function of channel delay τ, if a Gaussian pulse of bandwidth B was transmitted. The CDFs are obtained by averaging the instantaneous power delay profiles as defined in [11] over several hundred channel realizations. The CDF representation allows some intuition of how much pre-coding gain can be achieved for the measured channels. It is visible that up to a channel delay of $\tau \approx 50\,\text{ns}$ probability is not negligible that the channel still contains significant energy. This emphasizes potential PPP gains up to at least 6 pulses for LOS and NLOS scenarios. Also RMS delayspreads of the different regions have been evaluated as defined in [11]. Values span from $\sigma_\tau = 10.3\,\text{ns}$ for LOS to $\sigma_\tau = 17.4\,\text{ns}$ for NLOS, and are listed in the legend of Fig. 2.

On the left hand side of Fig. 3, the channel output of a NLOS CIR from ETHZ measurements is shown for a normalized Gaussian transmit pulse of bandwidth equal to $B = 2.9\,\text{GHz}$. The small points indicate which multipaths of the CIR are combined by the PPP pre-coder with $N_P = 4$. The corresponding pre-coded

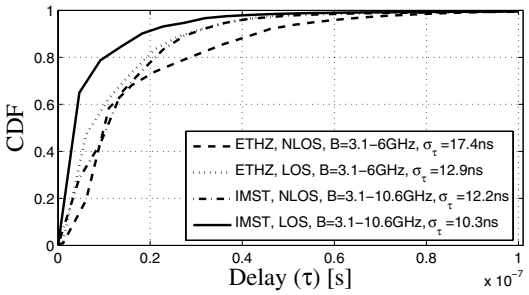

Fig. 2. CDF of CIR output energy plotted over channel delay of NLOS and LOS scenarios measured at ETHZ and IMST.

channel output, i.e., $\sum_{n=0}^{3} h_w(t-\tau_{p,n})$, is shown on the right hand side. In Fig. 3, a strong advantage of PPP pre-coding over

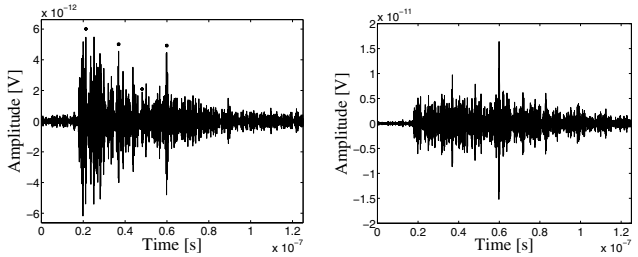

Fig. 3. Left: NLOS channel output for single Gaussian pulse of bandwidth $B = 2.9\,\mathrm{GHz}$. Right: Pre-coded channel output, if $N_p = 4$ is applied.

simple repetition coding is highlighted. The equivalent channel is not significantly more spread over time than the uncoded one. Hence, PPP has much smaller channel occupation time than a corresponding repetition code, i.e., $N_P \cdot \tau_c \gg \tau_c + (N_P - 1)T_{pc}$, with τ_c the channel excess delay. This is especially interesting for MAC layer, where the large silent times can be used by other users, e.g., in TDMA.

The SER curves presented are obtained by evaluating the energy collected by the SRAKE from the equivalent channels, i.e., $E_p \sum_{i=0}^{N_R-1} h_{E,i}^2$, and plugging this energy into (7). For all simulations, a Gaussian bandpass pulse $w_{tx}(t)$ of 10 dB bandwidth B is used, with $\int_{-\infty}^{\infty} w_{tx}^2(t)dt = 1$. For the SER curves, we apply a somewhat unusual SNR normalization. We normalize it to the total received energy, if a single pulse was transmitted, i.e., to $E_p \int_{-\infty}^{\infty} h_w^2(t)dt$. The reason for this is that in UWB, radiated power is not the dominant factor in system power consumption but is rigorously limited by power constraints[1]. Therefore, we plot the SER curves over $\zeta = \frac{E_p}{N_0} \int_{-\infty}^{\infty} h_w^2(t)dt$, i.e.:

$$P_e \quad = \quad \frac{1}{2}\,\mathrm{erfc}\left(\sqrt{\frac{\zeta \sum_{i=0}^{N_R-1} h_{E,i}^2}{2\int_{-\infty}^{\infty} h_w^2(t)}}\right). \qquad (15)$$

In Fig. 4, pre-coding gains are depicted for different scenarios measured at ETHZ (Left) and IMST (Right) with respect to single pulse transmission. Pre-coding gain is defined as the SNR gain (in dB) over the uncoded ($N_P = 1, N_R = 1$) scheme at a SER of 10^{-3}. Similar pre-coding gains are achieved for CIRs from ETHZ and IMST, pointing out that pre-coding performs well in different environments. Coding gains up to about 9 dB can be achieved. It is remarkable that pre-coding gain increases significantly up to six pulses, even for LOS scenarios. This was expected from observation of the CDF curves in Fig. 2, where we estimated PPP potential for up to 6 pulses. On the other hand, it is clearly visible from Fig. 4 that there is only little additional gain for 9 and more pulses, confirming intuition as well. It is noteworthy that pre-coding works similarly well for transmit pulses of bandwidth 500 MHz, 2.9 GHz and 7.5 GHz. Hence, we might rather decide for a UWB-IR system of 500 MHz than 7.5 GHz due to lower hardware requirements and decreased sensitivity to system uncertainties, as e.g., clock jitter.

[1]Plotting SER over receiver SNR cancels out pre-coding gains arising from higher transmit power.

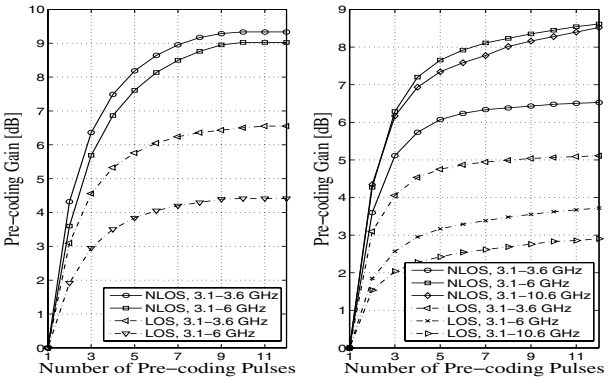

Fig. 4. Pre-coding gains for channels of different bandwidth measured at ETHZ (Left) and IMST (Right).

In Fig. 5, SER performance curves are plotted for varying numbers of pre-coding pulses N_P and SRAKE fingers N_R, if a transmit pulse of frequency range 3.1 to 3.6 GHz is sent over NLOS channels. Same channels have been used for evaluation of the CDF curve in Fig. 2, labelled as ETHZ NLOS. It is visible, that

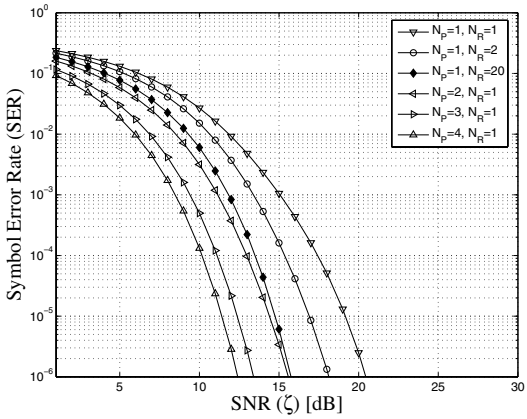

Fig. 5. SER performance for different numbers of PPP pulses N_P and SRAKE fingers N_R in a NLOS scenario.

PPP-BPPM with no more than two or three pulses in conjunction with a simple one finger SRAKE outperforms single pulse transmission combined with a 20 tap SRAKE. Two or three times more transmit power is used, but transmit power is not immediately the most dominating term of a UWB transmitter's power consumption and SRAKE fingers increase costs significantly as well, even if implemented digitally. For $N_P = 4$, the pre-coded main peak

that will be "selected" by the one finger SRAKE can be identified from Fig. 3 (Right). Note that the one finger SRAKE's clock can really be operated at frame repetition rate, i.e., $R_f \leq 300\,\mathrm{kHz}$, which leads to even higher decreased power consumption as well as cheaper hardware. We have demonstrated an efficient way to transform almost entire receiver complexity to transmitter side.

In order to gain some intuition of PPP scalability potential, we have plotted the SNR gain (in dB) at SER $= 10^{-3}$ over varying numbers of pre-coding pulses N_P and SRAKE fingers N_R. Thereby, SNR gain is defined with respect to single pulse transmission in conjunction with a one finger SRAKE, i.e., $(N_P = 1, N_R = 1)$ at SER $= 10^{-3}$. For NLOS, this is shown in Fig. 6. Two contour lines differ by $1\,\mathrm{dB}$ in SNR gain. Pairs

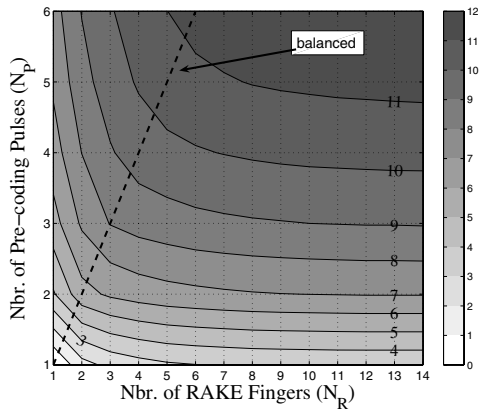

Fig. 6. SNR gain (in dB) at SER $= 10^{-3}$ for changing numbers of pre-coding pulses N_P and SRAKE fingers N_R, in NLOS scenario.

(N_P, N_R) lying on the same contour curve have the same gain and are interchangeable without changed SER performance. Pairs within the same region vary at most by $1\,\mathrm{dB}$ in SNR gain. In the region between 6 and $7\,\mathrm{dB}$, one finds (N_P, N_R) pairs, e.g., $(2, 8), (3, 2)$ and $(4, 1)$ of gain difference at most $1\,\mathrm{dB}$. In terms of Tx/Rx-scalability, we conclude that theses schemes are exchangeable with respect to SER performance, and we can therefore transform up to 6 SRAKE fingers into one additional PPP pulse by applying $(3, 2)$ instead of $(2, 8)$. Furthermore, a (2,1) system outperforms single pulse transmission in combination with a 14 finger SRAKE, i.e., (1,14). This shows above result from another point of view.

If we consider overall costs of additional PPP pulses and additional SRAKE fingers approximately equal, plotted contour lines in Fig. 6 clearly favor "balanced" systems over "unbalanced" ones, e.g., (3,3) over (1,14). It seems that systems with $N_R \gg N_P$ or $N_R \ll N_P$ waste resources against systems with approximately $N_R \approx N_P$. I.e., additional energy introduced by an additional pre-coding pulse, can almost entirely be collected by only a few additional SRAKE fingers.

5. CONCLUSIONS

A simple PPP scheme for LDR applications was proposed, directly derived from FCC-like power constraints, which requires only partial channel state information at transmitter side. It dictates minimal temporal pulse distance and maximal number of pre-coding pulses scaling with $1/\sqrt{R_f}$. Maximally achievable pre-coding gain as well as scalability potential of the scheme was demonstrated. It was shown that already two or three PPP pulses are sufficient to save many SRAKE fingers, ending up in significantly simplified receiver structures. Finally, it was shown that "balanced" systems with $N_P \approx N_R$ are more cost efficient than "unbalanced" ones.

6. ACKNOWLEDGEMENT

The authors would like to thank all partners of the PULSERS project (www.pulsers.net), that is partially funded by the European Commission and the Swiss Federal Office for Education and Science, for their contributions and constructive discussions.

7. REFERENCES

[1] J.R. Foerster, "Channel modeling sub-committee report final," Tech. Rep., IEEE P802.15 02/490r1–SG3a, Feb. 7, 2003.

[2] I. Oppermann, L. Stoica, A. Rabbachin, Z. Shelby, and J. Haapola, "UWB wireless sensor networks: UWEN - a practical example," *IEEE Commun. Mag.*, vol. 42, pp. 27–32, Dec. 2004.

[3] M. Chen and X. Li, "Transmitter-based channel equalization and MUI suppression for UWB systems," in *Int. Conf. on Mod. Prob. of Rad. Eng., Telecomm. and Comm. Science*, Slavsko, Ukraine, Feb. 24–28, 2004, pp. 501–504.

[4] K. Usuda, H. Zhang, and M. Nakagawa, "Pre-Rake performance for pulse based UWB system in a standardized UWB short-range channel," in *IEEE Wirel. Comm. and Netw. Conf. (WCNC)*, Atlanta, GA, Mar. 21–25, 2004, vol. 2, pp. 920–925.

[5] S. Imada and T. Ohtsuki, "Pre-RAKE diversity combining for UWB systems in IEEE 802.15 UWB multipath channel," in *Joint UWBST & IWUWBS*, Kyoto, Japan, May 18–21, 2004, pp. 18–21.

[6] T. Strohmer, M. Emami, J. Hansen, G. Papanicolaou, and A. J. Paulraj, "Application of time-reversal with MMSE equalizer to UWB communications," in *IEEE Proc. GLOBECOM*, Dallas, TX, Nov. 29 – Dec. 3, 2004, vol. 5, pp. 3123–3127.

[7] H. Sheng, A.M. Haimovich, A.F. Molisch, and J. Zhang, "Optimum combining for time hopping impulse radio UWB RAKE receivers," in *IEEE Conf. on UWB Sys. and Tech. (UWBST)*, Reston, VA, Nov. 16–19, 2003, pp. 224–228.

[8] FCC, "Revision of part 15 of the commission's rules regarding ultra-wideband transmission systems," *First Report and Order, ET-Docket 98-153, FCC 02-28*, adopted/released Feb. 23, 2004/Apr. 22, 2002.

[9] M. Weisenhorn and W. Hirt, "Impact of the FCC average- and peak power constraint on the power of UWB radio signals," Tech. Rep. D3b4b-Annexe, In PULSERS, Apr. 2004.

[10] F. Althaus, F. Troesch, T. Zasowski, and A. Wittneben, "Spatio-temporal signature measurement and characterization," Tech. Rep. D3b6a, In PULSERS, Dec. 2004.

[11] J. Karedal, S. Wyne, P. Almers, F. Tufvesson, and A.F. Molisch, "UWB channel measurements in an industrial environment," in *IEEE Proc. GLOBECOM*, Dallas, TX, Nov. 29 – Dec. 3, 2004, vol. 6, pp. 3511–3516.

[12] J. Kunisch and J. Pamp, "Measurement results and modeling aspects for the UWB radio channel," in *IEEE Conf. on UWB Sys. and Tech. (UWBST)*, Baltimore, MD, May 21–23, 2002, pp. 19–23.